Frictionless compression testing using load-applying platens made from porous graphite aerostatic bearings

Tarek El-Aguizy, Jean-Sebastien Plante,[a] Alexander H. Slocum,[b] and John D. Vogan
Massachusetts Institute of Technology, Room 3-455, 77 Massachusetts Ave., Cambridge, Massachusetts 02139

(Received 8 March 2005; accepted 17 May 2005; published online 29 June 2005)

In compression testing of soft materials at high strains, friction between a sample and the load-applying platens induces a differential lateral expansion that is visually evident as barreling. Barreling reduces the accuracy of the tests as a means of establishing accurate material properties. Current techniques for reducing friction, which involve liquid squeeze film lubrication, may not achieve true frictionless interfaces, are messy, and may adversely affect some samples. This article examines the use of porous graphite aerostatic bearings as a frictionless testing interface. The physics of a soft material under compressive loading by porous air bearings is investigated with simple finite element analysis and air flow models. An aerostatic bearing assembly is also constructed and compared to other friction reduction techniques. The results of these experiments indicate that there are benefits to using air bearings as they are clean, chemically inert, extremely stiff, reduce friction to levels comparable to existing methods, have negligible squeeze film effect, are repeatable, and allow for cyclic compression testing. © *2005 American Institute of Physics.* [DOI: 10.1063/1.1949467]

I. INTRODUCTION

Within the realm of material testing, compression and tension tests are most frequently performed to determine material properties. In compression testing, particularly for soft materials that undergo high strains, friction between the sample and the load-applying platens deforms the sample nonuniformly giving it a characteristic barrel-like shape. Such barreling can significantly affect the measured material properties and reduce the efficacy of testing as a means of observing true material properties. Current techniques for reducing the friction between platens and test samples include the use of liquid lubricants such as oil or soapy water. However, both of these techniques may not effectively achieve true frictionless compression testing and are somewhat messy. Moreover, the effect of the lubricant on some soft materials may adversely change the mechanical properties. Porous graphite aerostatic bearings, used in a variety of precision machine applications,[1] provide a potentially useful method for reducing interface friction.

The goal of this research was to design a compression testing system that integrates porous aerostatic bearings as the loading surfaces, and to compare the relative stress/strain characteristics of this frictionless system to standard friction reduction methods. To aid in this process, the functional requirements for frictionless compression testing were reviewed and each alternative was evaluated against these requirements. Along with a conceptual evaluation, an aerostatic bearing assembly was constructed and multiple experiments were performed to characterize the air bearings' performance. Other friction reduction methods were characterized as a means of benchmarking the merit of using aerostatic bearings in compression testing.

In the following subsection, the mechanics of material testing are briefly described to clarify the motivation for this investigation. In Sec. II, the air bearing/sample interface is evaluated analytically and the bearing/sample interface is modeled using finite element analysis (FEA). Section III reviews the setup, design, and specifications of the frictionless testing system. Section IV presents the results of multiple tests characterizing aerostatic bearing performance across several domains of performance. Section V is a discussion of the merit of porous media aerostatic bearings and their applicability for various uses, as well as suggestions for further work in this area.

A. Motivation

When a material is subject to a uniaxial stress, a strain in the direction of the stress will cause a strain in the orthogonal direction via the Poisson effect, so that $\varepsilon_2 = -\nu\varepsilon_1$, where ν is the Poisson ratio. The ideal case is shown in Fig. 1(a). For typical compression testing, however, there is friction at the interface of the sample and the platen applying the force. This friction imposes a shear stress on the interface that inhibits the sample's lateral expansion. The interface shear stresses cause localized deformation near the faces of the sample, creating a bowed shape similar in shape to a barrel, as shown in Fig. 1(b).

For soft elastomeric materials, with Young's moduli below 1 MPa and Poisson ratios near 0.5, engineering strains can exceed 50%. At such high deformations, the barreling effect is significant and reduces the cross-sectional stress dis-

[a]Author to whom correspondence should be addressed; electronic mail: jsplante@mit.edu
[b]Electronic mail: slocum@mit.edu

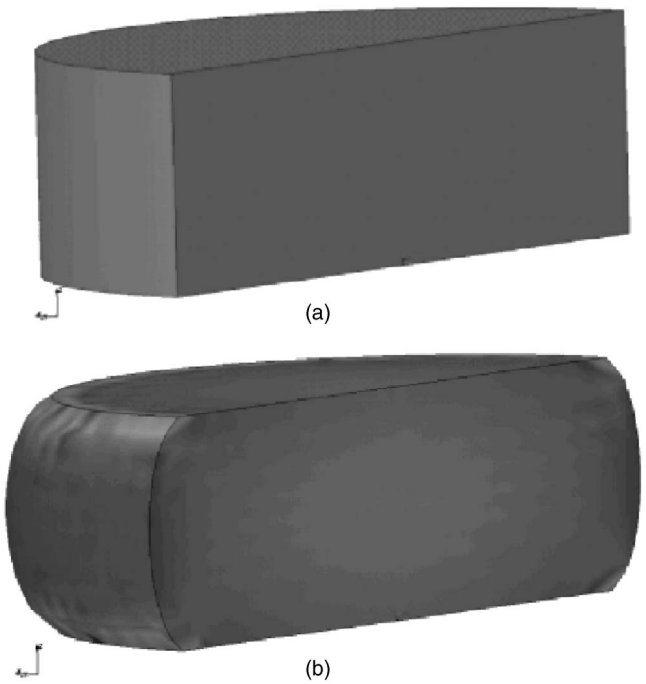

FIG. 1. Ideal (a) and typical (b) compressed samples.

tribution uniformity. This can lead to substantial errors when trying to accurately infer material properties from experimental data. Accordingly, the primary benefit of reducing the friction at the interface between the platen and the material is to prevent any differential strain buildup in the sample, thereby allowing the material to maintain its cross-sectional uniformity.

Currently, the primary method for reducing friction is to lubricate the surface between the sample and platen with a liquid, typically oil or soapy water. These methods require the user to apply the lubricant and are messy, potentially incompatible with some materials, and may degrade in performance during cyclic tests. Further, it is unclear whether these methods partially or fully eliminate the effects of friction on test samples. Accordingly, this investigation develops a friction reduction technique that avoids some of the issues of current methods used for frictionless material testing, while at the same time benchmarking the performance of the current methods.

II. ANALYTICAL DEVELOPMENT

A. Measurement of material properties

The commonly used parameters to represent stress and strain are the engineering stress and strain:

$$\sigma = \frac{F_A}{A_0}, \qquad \varepsilon = \frac{\delta}{l_0} \tag{1}$$

where F_A is the force applied to a sample face; A_0 is the initial area of sample face; δ is the incremental change in sample length; and l_0 is the initial length of a sample.

For soft materials that undergo large deformations ($>10\%$), stress and strain should account for the change of sample shape during the deformation. In this case the true stress and true strain concept as defined in Eqs. (2) should be used:

$$\sigma = \frac{F_A}{A_i}, \qquad \varepsilon = \ln\frac{l}{l_0}, \tag{2}$$

where A_i is the instantaneous area of sample face and l is the instantaneous length of a sample.

True stress is defined using the instantaneous area of the sample as opposed to only considering the initial area. Similarly, true strain, which is based on the sum of incremental strains, is the preferred definition when a material undergoes large strains as well as when plotting true stress.[2] The slope of a true stress-true strain curve within the elastic regime provides the true value of the Young's modulus. For soft materials such as the silicone rubber used in this study, typical moduli are on the order of 300 kPa.

Most soft materials, such as polymers and biological tissue, behave nonlinearly at high strains. In such cases, the material properties are not defined by a single value of Young's modulus. For comparing data sets, therefore, it is more useful to examine the slope of the entire curve. A plot of the slope, or "instantaneous modulus," $\partial\sigma/\partial\varepsilon$, directly shows how the modulus of the material is changing as function of stress and strain.

The testing method that induces the least amount of friction in the system is the one that will most accurately represent the true properties of the material. This is due to the fact that interface friction tends to constrain and apparently stiffen a sample.

B. Porous air bearing operation

Air bearings normally run with very small air gaps between the bearing and bearing ways, normally between 5 and 10 μm.[3] Such small gaps require very smooth surfaces when the bearing runs on rigid ways. The main reason for such small gaps is to realize reasonable flow rates. Small gaps are undesirable for material testing because an ideal testing machine should not be limited by surface finishes.

A simple one dimensional (1D) compressible flow model was used for understanding the impact of the bearing gap on air bearing operation.[4] The 1D model was used to study a circular air bearing of 24.1 mm in diameter riding on a flat surface under a 50 N load and 414 kPa supply pressure.[4] Empirical relations were developed between bearing performance metrics (bearing gap h, air mass flow rate $\dot{m}$, stiffness K), and the main design parameter (permeability ratio, k_y/H)[4]

$$h = 4.36 \times 10^5 \left(\frac{k_y}{H}\right)^{0.3829}, \tag{3}$$

$$\dot{m} = 3 \times 10^7 \left(\frac{k_y}{H}\right), \tag{4}$$

$$K = \frac{\partial F}{\partial h} = 818.6 \left(\frac{k_y}{H}\right)^{-0.3159}. \tag{5}$$

In Eqs. (3)–(5), the exponent of the permeability ratio term illustrates the relative strength of the design parameter on performance metrics. Comparing Eqs. (3) and (4) reveals

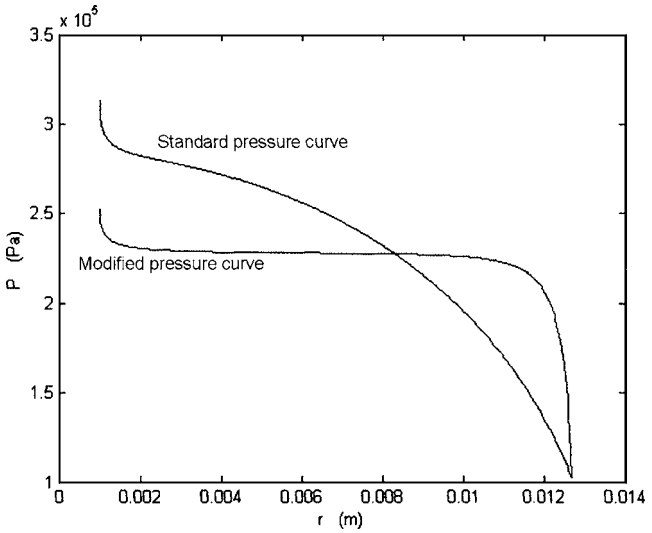

FIG. 2. Theoretical pressure profile, 50 N load at 60 psi.

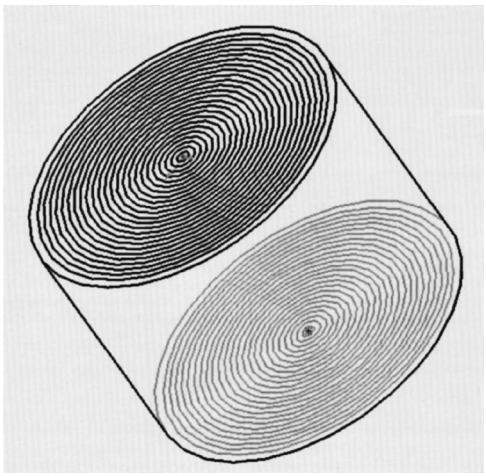

FIG. 3. Solid model of sample with concentric faces to enable FEA to apply different pressure profiles.

that the bearing gap can only be increased with a significant penalty in mass flow. High air flow penalties are tolerable because testing is an intermittent activity.

The negative exponent of Eq. (5) shows that the bearing gap stiffness decreases with increasing permeability ratio. However, a 100× increase in permeability ratio only reduces the stiffness by a factor of 4.3. Since air bearing stiffness is much stiffer than elastomer samples, $\sim 10^9$ N/m (Ref. 4) versus $\sim 10^5$ N/m, the bearing stiffness has a negligible influence on measurements, even for very high permeability ratios.

Hence we can conclude that the concept of using specially designed air bearing with high permability ratios to maximize the bearing gap is feasible.

C. FEM of bearing/sample interface

Theoretical analysis shows that porous media aerostatic bearings create a nonuniform pressure profile on their loading interfaces. An unloaded bearing has a uniform flow across the entire bearing face, whereas applying a load on either a portion or all of the bearing face will result in a change in the uniform air flow and create a particular pressure profile computed via the 1D model discussed above.[4] Such a pressure profile, an example of which is shown as the standard pressure curve in Fig. 2, results from the porous nature of the bearing, the loads, and the boundary conditions imposed on the bearing interface.

A elastomer material loaded by such a nonuniform pressure should exhibit some amount of interfacial deformation. When the material does start to deform there should be a corresponding change in the pressure profile, resulting in some equilibrium deformation governed by the material stiffness and the bearing properties.

A linear finite element model of cylindrical Dow Corning HS-III silicone (the selected soft rubber used for experimentation within this investigation) samples subject to nonuniform compressive loading was created to investigate the potential interfacial deformation of soft material samples. The model sample is a 25.4 mm (1.0 in.) diam plug with a height of 19 mm (0.75 in.), the size of one of the actual samples used in testing. A solid model of the sample was created in SOLIDWORKS® and analyzed with COSMOSWORKS®. To model the nonuniform pressure profile, the sample faces were split into 25 concentric rings, with radii incrementally increasing by 0.5 mm, except for the outermost ring which spans from 12.0 to 12.7 mm. To prevent the rings from merging into a single face, each ring is slightly higher than its larger neighbor by 1×10^{-4} mm, which is 3 orders of magnitude smaller than the observed strains and a small enough difference to be negligible for the FEA results. The resulting solid model is shown in Fig. 3.

The material properties used in the FEA are a Young's modulus of 300 kPa and a Poisson ratio of 0.49, values similar to those for HS-III. The pressure profile used on each of the 25 faces is consistent with that shown earlier in Fig. 2, subtracting out atmospheric pressure so the FEA solves only for incremental loads. Frictional shear stresses on the sample face due to radial flow were neglected. Identical pressure profiles are applied on the top and bottom faces. A view of the element absolute displacement for the sample is shown in Fig. 4(a). As is observed in the plot's dispersion, the nonuniform loading does cause significant relative deflection between the center and perimeter (edge-to-center) of the sample face. At nearly 2 mm of edge-to-center deflection, this result clearly indicates that the peaked pressure profile of Fig. 2 is not a realistic loading scenario.

In reality, the expected pressure distribution shifts as the sample bows, and the final expected displacement should be obtained by iterating between the analytical solution of the pressure profile (which depends on the sample bow) and the

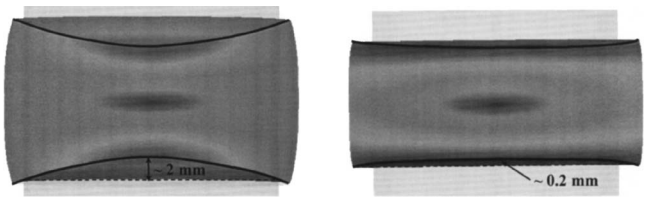

FIG. 4. FEA displacement plots on a cross-sectional view of a cylindrical sample loaded with; (a) original pressure profile and (b) modified pressure profile.

TABLE I. Design development concept matrix.

Concept	Physics/Analytics of operation	Benefits	Risks/Drawbacks
Air–porous media	Pressurized air flow through porous material	Clean, flexible sample sizes	Expensive, setup requirements
Air–orifice	Pressurized air flow through a finite set of orifices	Clean	Hammering, instability, setup
Hydrostatic	Oil-based bearing	Standard technology	Messy, material compatibility
Oil	Oil load-bearing layer	Ease of use	Messy, material compatibility
Expandable membrane	Membrane flexible in lateral direction while applying force	No chemical interactions	Vertical stiffness, lateral strain matching, sourcing
Surfactant	Liquid phase lubricant layer between platen and sample	Ease of use	Messy, material compatibility
Teflon surfaces	Solid phase lubricant between platen and sample	No chemical interaction	Stretch characteristics, high friction
Electroactive	Membrane between platen and sample expands with voltage	No chemical interaction	Lateral strain matching, calibration and sourcing
Expandable platen	Platen surface geometry mechanically expands	No chemical interactions	Complexity, lateral strain matching

FEA solver (which depends on the pressure profile). Accordingly, the analytical air-flow model of an air bearing was modified to include the effects of surface deflection from the bearing center to exit edge. A corresponding pressure profile is shown in Fig. 2 as the modified pressure profile, and is significantly flatter than the standard pressure profile.

The modified pressure profile was then used in a second FEA iteration round that lead to the displacements shown in Fig. 4(b); the resulting edge-to-center deflection is measured using the FEA probe function to be approximately 200 μm. This result supports the flatter modified pressure profile as a more realistic pressure distribution for soft materials, reducing the edge-to-center deflection from 2 mm to 200 μm. Further refinement of the two models would likely narrow this difference, but is not within the scope of this article. As an example, using the true shape of a bowed sample instead of a linear approximation in the 1D model would produce an even flatter pressure profile. The true shape has a larger pocket gap which implies that all the flow restriction needs to occur suddenly at the bearing edge. Thus, the pressure distribution is closer to a perfectly flat one where the inside pocket of the sample is filled with constant pressure. This converging mechanism is a demonstration of the self-help principle:[3] the more the sample bows, the flatter the pressure distribution, and the bowing rate decreases. An equilibrium point therefore occurs at a much smaller edge-to-center deflection than predicted using the pressure profile for rigid ways.

Loading of an HS-III sample with 50 N of force induces an average deflection of 4.8 mm for the geometry mentioned above. The 50 μm edge-to-center deflection predicted by the 1D model is taken as a typical soft material deflection and corresponds to $2\times0.05/4.8=2\%$ of the average length change, which is not significant. Further, the observed material properties measured using air bearings and other frictionless techniques such as a soapy water layer are almost identical, which indicates that any interfacial curvature has no significant effect on the observed properties.

III. EXPERIMENTAL SYSTEM

A. Design concept review

Various concepts for frictionless force interfaces were evaluated, and are shown in Table I. The concepts based on porous aerostatic bearings, orifice bearings, and hydrostatic bearings entail the mounting of the bearings onto the platens of an existing testing machine. Oil and surfactant (soapy water) refer to the use of a liquid between the sample and the platens. This requires the user to manually apply a liquid between the sample and platen immediately prior to testing, and is the current method recommended by ISO 7743 for frictionless testing.[5] The Teflon surfaces concept uses Teflon sheets applied between samples and platens; this technique by itself does not significantly reduce friction and is thus often used in conjunction with oil or surfactant lubrication. The expandable membrane, expandable platen, and electroactive concepts are similar in requiring the platen to grow in the lateral direction to match the expansion of a sample. The expandable membrane is a stretch membrane that is stretched by the expanding sample; the expandable platen can either passively deform mechanical members or actively deform to match lateral strain; and the electroactive method actively matches the lateral strain of the sample.

Each concept is evaluated on the basis of the following functional requirements: measurement precision, cost, manufacturability/availability, reliability, and flexibility. The strain matching, or expandable, concepts were eliminated early in the selection process as being unlikely of succeeding and excessively complex. Hydrostatic bearings were considered, but were rejected because they are messy. This leaves aerostatic bearings, either orifice or porous media based, as well as current oil or surfactant lubrication. Accordingly, bench level experiments were run to establish the performance of orifice and porous media aerostatic bearings and aid in selecting one of the two concepts.

For the initial experiments, square and cylindrical samples molded from a HS-III silicone rubber were tested

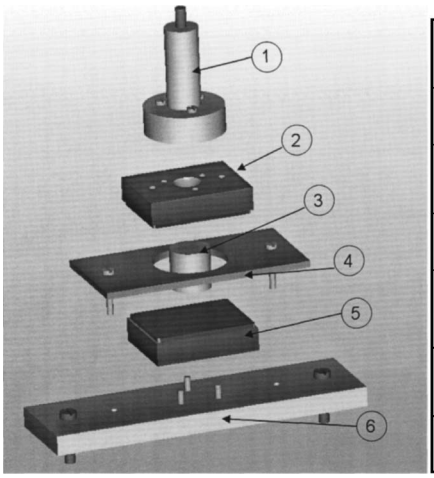

Assembly Components	
1	Top Fixture
2	Air bearing platen
3	Sample
4	Sample lateral restrainer
5	Air bearing platen
6	Bottom plate

FIG. 5. Fixturing assembly components.

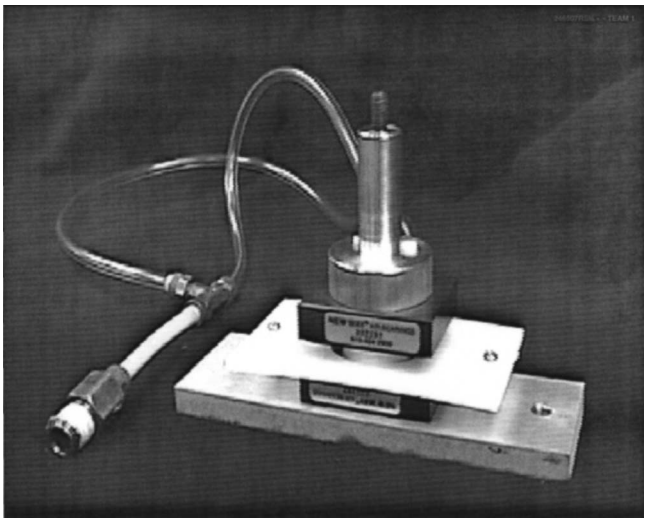

FIG. 6. Test setup for using air bearing interface.

using a custom-made orifice bearing and a porous graphite aerostatic bearing. Both bearing types experienced a vibratory response. Sound intensity measurements have shown that the response for the porous media bearing is significantly lower (at least 15 dB) than the response of the orifice bearing, especially at higher frequencies.

The vibration problem observed is not a classical pneumatic hammering problem where the bearing is in relative motion with respect to a fixed and rigid bearing way; a compliant interface changes the entire bearing system dynamics. One potential explanation of this resonant behavior is that the sample's free modes of vibration are aerodynamically excited by the air flow. This explanation was verified by solving the classical continuous model of a free-free rod in compression with the sample parameters. The numerical values of the first three resonant frequencies coincided almost exactly with the first three experimental peaks.

Porous media bearings were selected over orifice bearings because of their better damping, more uniform pressure profile, and indifference to the sample location relative to the bearing center.

B. Fixturing assembly

Air bearings are often mounted on spherical joints to allow for nonparallelism of the surfaces. For material testing, this may present difficulties if the compressive load is not exactly aligned with the sample's center of stiffness. In this case, the moment created by the misalignment will cause the bearing to tilt and the sample will be forced to one side. Therefore, in this study, the air bearing platens were mounted rigidly to eliminate this unstable situation.

An exploded view of the fixturing assembly is shown in Fig. 5. The fixtures (components 1 and 6) are machined from 6061 aluminum. The top component attaches to the upper beam of any tensile testing apparatus and the bottom plate attaches to the base of the machine. The number of components was minimized to limit parallelism errors. The machined fixtures proved to be more precise than the original setup, with a final parallelism error well below the targeted 0.5° mark. The center piece (component 4) is a lateral restraint device for assuring that the sample does not slide out from between the platens. Even with minimized parallelism errors and very small side loads, friction is so low that a sample could easily slide out of the system.

New Way Precision, Inc. 40×50 mm porous graphite bearings (S124001) were used for the frictionless force interfaces. These bearings' pads are large enough to accept a variety of samples. The force/displacement characteristics of the bearings were provided by the manufacturer.[6] According to these specifications, the typical gap of the bearing during soft material compression will vary from approximately 5 to 20 μm. This distance is about 3 orders of magnitude smaller than the expected deformation of the sample, so the changing thickness of the air gap will have an insignificant effect in the displacement data.

IV. EXPERIMENTAL RESULTS

A. Testing procedure

Experiments were conducted under a variety of conditions to allow for comparison to conventional testing methods. The various surface interfaces used were air bearings (at pressures of 60–100 psi), soapy water (about 15% concentration of hand soap), silicone oil (10 W), and dry (no fluid lubrication). For the air bearings tests, a custom assembly, shown in Fig. 6, was mounted to the testing machine. For the dry tests, the sample was set directly on an air bearing pad with zero input pressure, with friction between the sample and graphite causing resistance to lateral expansion and obvious barreling. For the liquid-lubricated interfaces, thin Teflon sheets were coated with the liquid and then placed between the platens and the sample to decrease friction as much as possible. For these tests, the custom air bearing assembly was replaced with the testing machine's standard aluminum platens.

HS-III silicone rubber was used for all samples. This elastomer is sold as a two part mixture that cures at room temperature in about 24 h. The samples were prepared in a controlled manner using the mold discussed in the previous section, which allowed control over sample size and surface roughness.

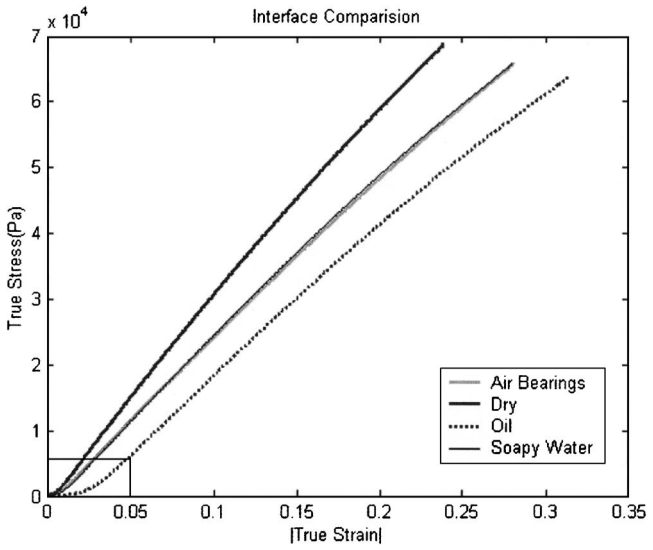

FIG. 7. Typical true-stress/true-strain data.

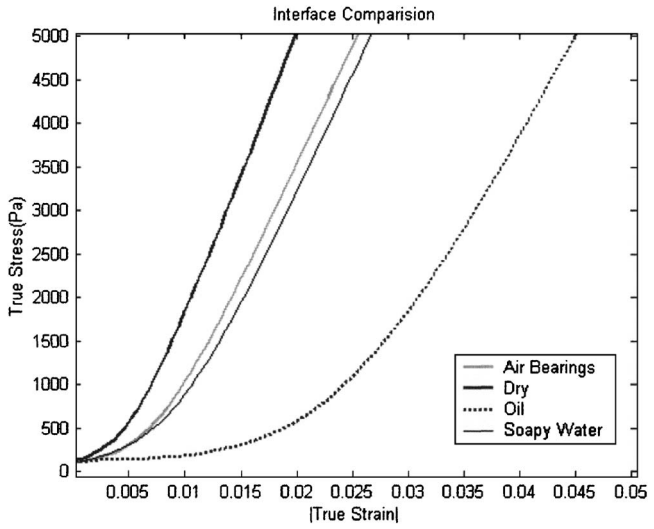

FIG. 8. Magnified view stress/strain plot, showing the squeeze film effect for each interface.

Using the setup described above, a series of single cycle compression tests were conducted on a variety of samples. Initial tests with HS-III silicone rubber have shown this particular elastomeric material to be repeatable enough to not require mechanical conditioning. Several different issues were studied during experimentation, including the impact of using liquid lubricants and any potential squeeze film effects, the impact of sample surface finish, the impact of sample geometry and aspect ratio, as well as the effect of cyclic tests. Several tests were repeated with a higher number of cycles (10–100 cycles) to identify any effects of cyclic testing on interface conditions.

A high precision material testing machine, the TA.XT Plus from Texture Technologies, was used for all tests. It has a 0.1 g resolution for force measurements and 0.001 mm resolution for displacement measurements. Measurement errors were considered insignificant due to the high accuracy of the machine and error bars are left off of the plots for clarity.

B. Squeeze film effects

Figure 7 and its closeup on Fig. 8 demonstrate typical true-stress/true-strain results comparing the various interfaces (the absolute value of true strain is used in all figures). Figure 9 shows the slope of the stress-strain curve as a function of true strain. In a perfectly linear-elastic model, this plot would be a horizontal line, occurring at the Young's modulus of the material. For the nonlinear, viscoelastic material being tested, this curve represents an instantaneous "modulus."

Figure 7 indicates that oil exhibited significantly lower stresses at any given strain than other testing methods; at a strain of 0.1, there is a 25% difference in recorded sample stress between the oil and air bearings/soapy water. However, the plot of the instantaneous slope (Fig. 9) indicates that the stiffness is not significantly different across methods, with only a 4% difference between the instantaneous moduli at a strain of 0.1. Accordingly, while oil does show slightly lower stiffness, the difference across frictionless interface methods is not as significant as the stress-strain plot initially suggests. The major difference shown in Fig. 7 is attributed to the squeeze film effect. This effect is apparent when looking at a magnified section of the stress/strain plot, as shown in Fig. 8.

When compressing a material with a liquid-lubricated interface, a liquid film is trapped between the sample and the platen surface. The bulk of this liquid is initially squeezed out of the gap with a small force, leaving a thin film that remains relatively consistent and provides lubrication for higher forces. Since the squeezed films and sample are in series, the squeeze film effect causes an apparently lower stiffness in the material. This is particularly noticeable at lower strains during initial loading where the film stiffness is lowest. Soapy water also shows the squeeze film effect, which is visible in Fig. 8, but it is much less significant for water since the viscosity is significantly lower. Air bearings also have a fluid (air) gap, but this gap is generally much smaller than for liquids, so that the air bearing appears stiffer

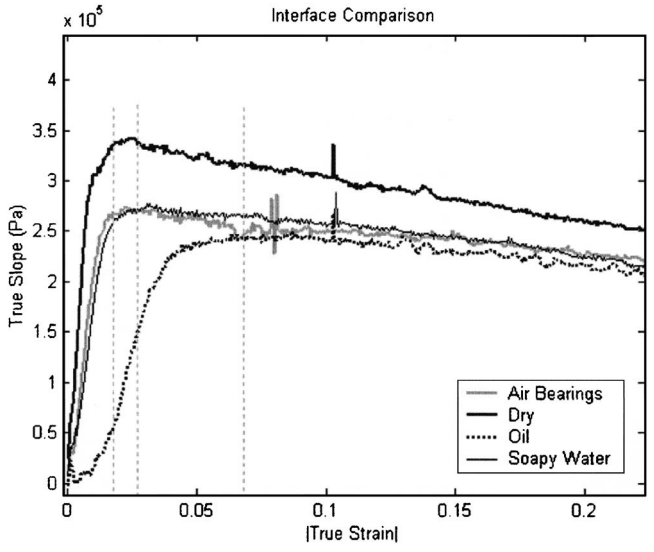

FIG. 9. Slope of true-stress/true-strain plot.

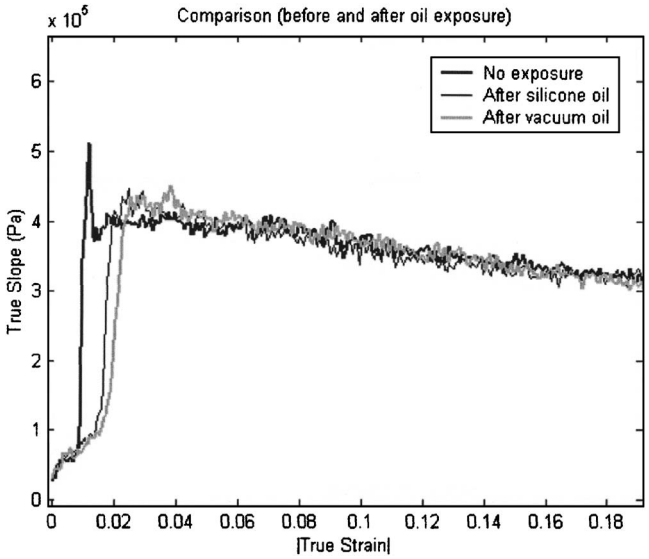

FIG. 10. Materials stiffness (dry conditions) both before and after exposure to oil.

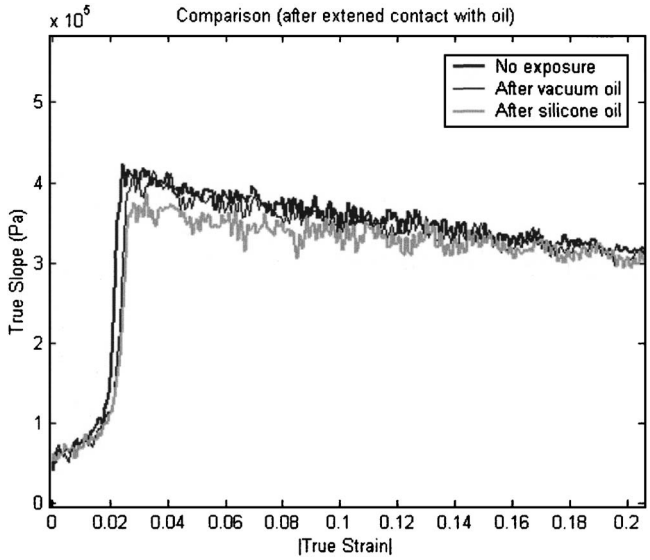

FIG. 11. Materials stiffness (dry conditions) both before and after repeated exposure to oil.

than the material being compressed throughout the loading phase.

Another issue to mention is "settling strain." This is the strain value where the instantaneous slope settles into a stable regime. Figure 9 shows this effect, with settling strains of 0.02 for air bearings, 0.03 for soapy water, and 0.07 for oil (each indicated in the figure). This indicates that there is a relative offset of the data due to the initial thickness of the liquid film. The position of this point is highly dependent on the viscosity of the lubrication fluid. The squeeze film effect is often negligible for soapy water, as shown above, but can vary significantly with the concentration of soap. Discrepancies in measurements due to the squeeze film effect can be neglected by shifting the data by the displacement indicated by the settling strain, but this value is not always clearly indicated.

It was suggested that the lower apparent stiffness yielded by oil tests might be due to actual material softening due to chemical reactions with the oil. To test this hypothesis, a separate sample was tested five times with the following conditions: (1) dry, (2) lubricated with silicone oil, (3) dry, (4) lubricated with pump oil, (5) dry. The slope-strain curves of the three dry cases are shown in Fig. 10. Ignoring initial differences due to changing boundaries, there is no visual difference between the stiffness profiles throughout the sample. Similar tests on another sample, however, showed possible shifts in stiffness, as shown in Fig. 11. Each of these tests were repeated, and the samples were exposed to oil for longer amounts of time. In all previous tests, the oil was washed off of the surface immediately. If chemical reactions were time dependent, then this might explain the shift in stiffness. It should also be mentioned that the sample used for these plots was cycled several times, and the apparent shift could also be a result of natural material softening that arises from cyclic testing. This is further supported by small shifts in the stiffness for consecutive tests when no oil has been applied.

During all other testing, exposure to oil was kept to a minimum and softening of the material due to repeated use would not be significant. It has therefore been concluded that, at the testing scale, the apparently lower stiffness obtained from oil lubricated tests is a result of a frictional interface change and not an actual material softening phenomena.[7]

C. Sample aspect ratio

Tests were performed to analyze the effect of the sample aspect ratio on test results. Figure 12 shows the slope-strain profile for three different samples, each with the same thickness, roughness, and composition, but with varying diameters (1.0, 0.75, and 0.5 in.). The largest sample yielded a slightly lower stiffness than the midsized sample, which yielded a lower stiffness than the smallest sample, suggesting that the method is more effective for larger diameters. This contrasts with compression testing methods with significant friction where, for constant thickness, the apparent material stiffness increases with sample diameter.[8]

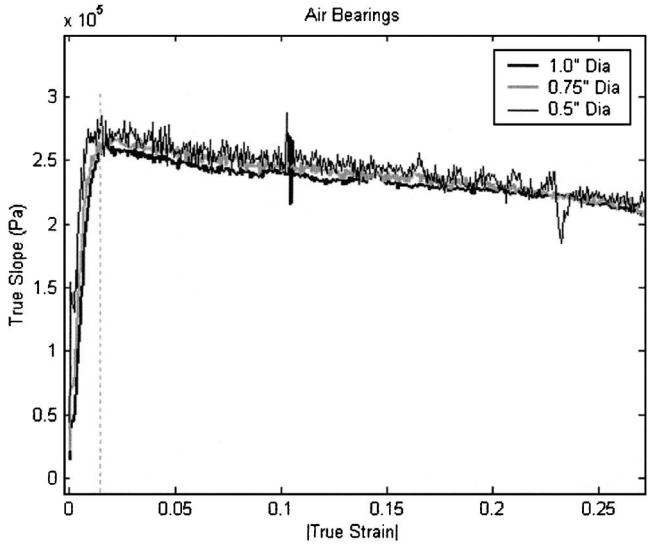

FIG. 12. Apparent stiffness with varying diameter (air bearings).

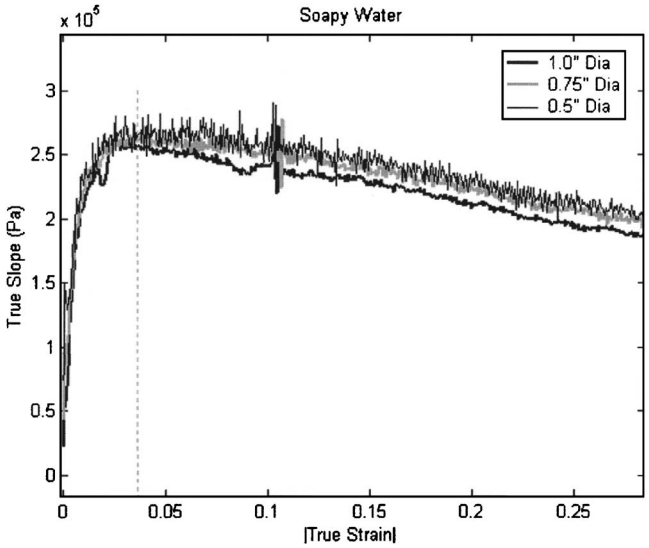

FIG. 13. Apparent stiffness with varying diameter (soapy water).

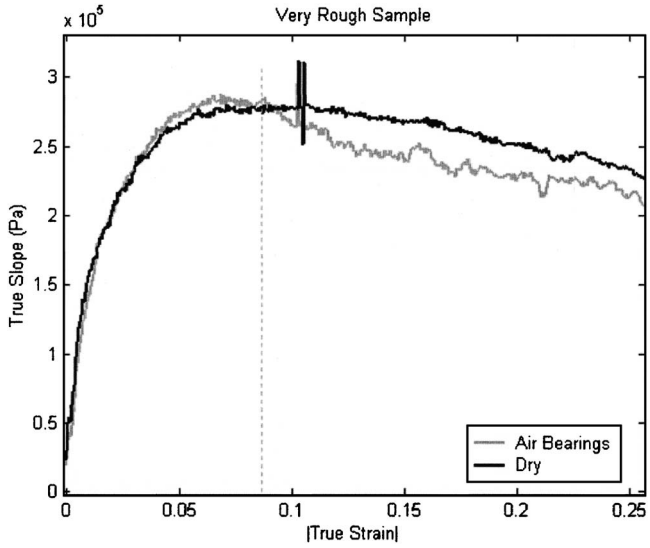

FIG. 14. Comparison of dry and pressurized cases for moderate roughness.

The reasons for the trend of decreasing stiffness with increasing diameter shown in Fig. 12 are not clear. The results suggest that air bearings become more efficient in eliminating friction as sample size increases. Assuming that friction occurs primarily at the edges of the sample (due to nonuniform pressure distribution), then edge-effect induced friction would be greater for smaller samples. The perimeter/area ratio is inversely proportional to the radius, so edge effects are more significant for smaller radii.

The trend of decreasing stiffness with increasing diameter is not exclusive to air bearings and is also observed with liquid lubrication, as shown in Fig. 13 for the case of soapy water. Here again, the results suggest that liquid lubricants become more efficient in eliminating friction as sample size increases. Again, this could be explained by the sample's perimeter/area ratio. The outlet for lubricant to escape (at the perimeter) becomes relatively smaller for larger samples. It may be possible that more fluid is trapped beneath the sample, causing less friction.

For both air bearings and liquid lubrication, further studies for determining the exact dependence of apparent stiffness on the size ratio of the sample are required.

D. Surface roughness

The effect of surface roughness on material stiffness testing was investigated. Typically, air bearings require very flat and smooth surfaces in order to maintain a stable air gap. For soft material interfaces, the required surface finish has not been established.

A specific case in which the surface was very rough was examined. The sample was cast directly onto the surface of 50-grit sandpaper, yielding a coarse, bumpy finish. Figure 14 shows a comparison of the dry and pressurized cases. Initially, there is no significant difference between the curves. At a strain of about 0.09, the curves seem to diverge and stiffness for the pressurized case drops below that for the dry case. This is most likely due to the relatively soft surface of the large asperities and their ability to flatten under compressive load. An air gap can then form locally under the asperities and friction is reduced significantly, thereby reducing the apparent stiffness (about 15%).

This phenomenon is verified at other roughness levels. Figure 15 shows the slope-strain profile of a sample molded on 80-grit sandpaper (less rough). Again, for low strains, the asperities dominate both cases until a certain threshold when the air bearing becomes better. For this case, the divergence occurs at a strain of 0.065. For the rougher sample, divergence occurs at a higher strain of about 0.09, as would be expected.

To compare how the air bearing performs relative to other lubrication methods at these very rough surfaces (with respect to relative stiffness), the same sample was tested with each method and the slope was graphed, as shown in Fig. 16. The large ramp up time for each case is most likely due to the surface bumps, which have a lower stiffness than the bulk section of the sample, being initially compressed. Each situation seems to settle into a linear regime at a strain of

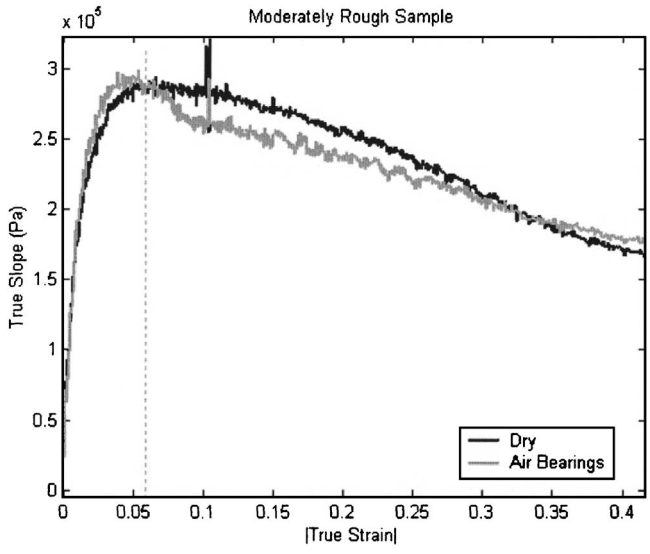

FIG. 15. Comparison of dry and pressurized cases for very high roughness.

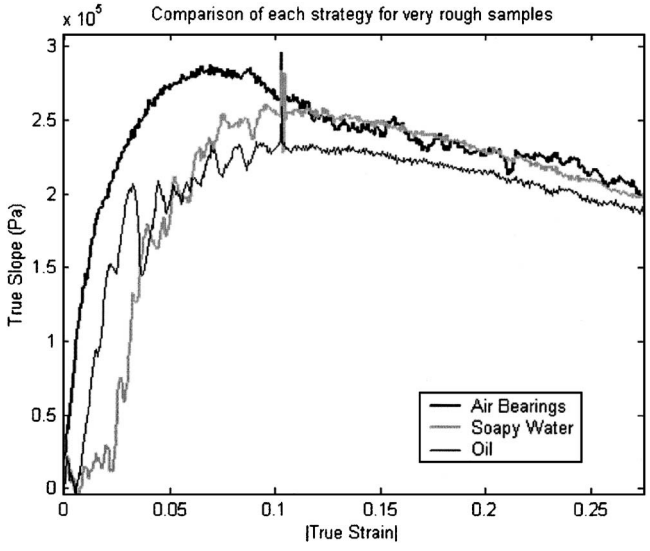

FIG. 16. Comparison of various interface conditions for very rough samples cast on 80 grit sandpaper.

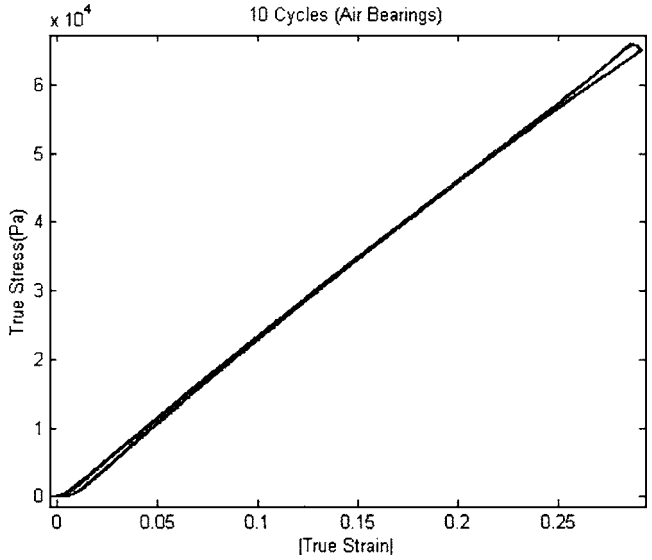

FIG. 18. Ten cycles with air bearing platens.

about 0.1. The results are typical: soapy water and air show almost the same behavior and oil is lower.

For more typical conditions, the samples would most likely be much smoother. To test the effect of moderate roughness, samples were cast onto metal caps with three different finishes: roughly sanded with 80 grit sandpaper, finely sanded with 300 grit sandpaper, and polished. The slope-strain curves, shown in Fig. 17, are almost identical, especially at low pressures. A slight divergence can be seen at a strain of around 0.20. After this point, the air bearing seems to perform better for smoother samples. This demonstrates that smoother samples performed slightly better at higher pressures. This can be attributed to fine asperities coming in contact with the bearing at higher pressure: fine asperities are now larger than the gap, which should be on the order of 10 μm.

These results imply that there are two different regimes of surface roughness: coarse and fine. For fine roughness, higher air flow rates are required to keep a sufficiently large gap to make the air bearing effective. That is, the gap must be large enough to accommodate the surface finish of the sample and the bearing as well as an unobstructed fluid film. Coarse roughness can, however, only be flattened to a certain extent, until fine roughness starts to degrade the performance as asperities contact the bearing surfaces at higher pressures.

The results obtained are meant to qualitatively show that standard testing procedures for air bearing compression testing should specify the surface roughness of the sample interface, and smoother is better. As discussded in Sec. II B, the minimum surface roughness would be dependent on the permeability ratio of the porous material, k_y/H. For the bearings used in the present study, a surface roughness (Ra) on the order of 1 μm, a value easily obtained with conventional machining processes, may be appropriate.

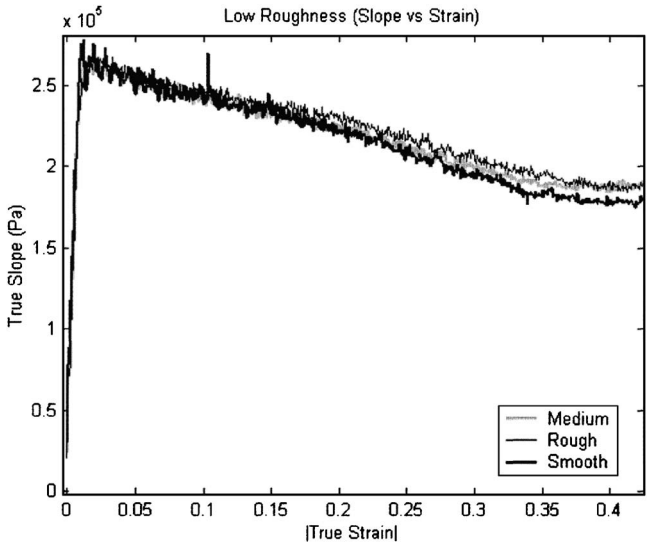

FIG. 17. Apparent stiffness for varying sample roughness on air bearing platens.

E. Cyclic conditions

The effect of cyclic testing on the surface interface (and vice versa) was investigated. Figure 18 shows a stress-strain plot for the air bearing interface recorded over ten cycles. There is a slight downward shift, as shown by Fig. 19. This shows the expected effect, where there is an actual softening of the material due to repeated cycles.

A similar test was repeated for 100 cycles with a soapy water interface. The stress-strain plots for cycles 1, 25, 50, 75, and 100 are shown in Fig. 20. A shift occurs in the direction opposite to the air bearing test. The effect is significant when comparing slope-strain profiles, as shown in Fig. 21. The slope (measured at a strain of 0.1) has increased about 10% over 100 cycles. Assuming this is not a material effect, the cause is most likely to be drying of the liquid interface. The actual change of the material properties is being masked by the changing interface conditions. Previous tests for similar samples show that dry interfaces appear about 15%–20% stiffer than lubricated interfaces. After 100 cycles, the curve has moved over half that difference.

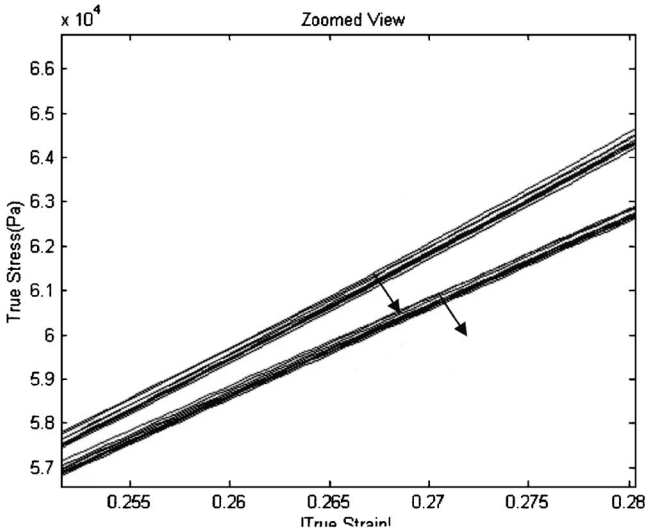

FIG. 19. Magnified view showing slow softening of material during cyclic tests with air bearing platens.

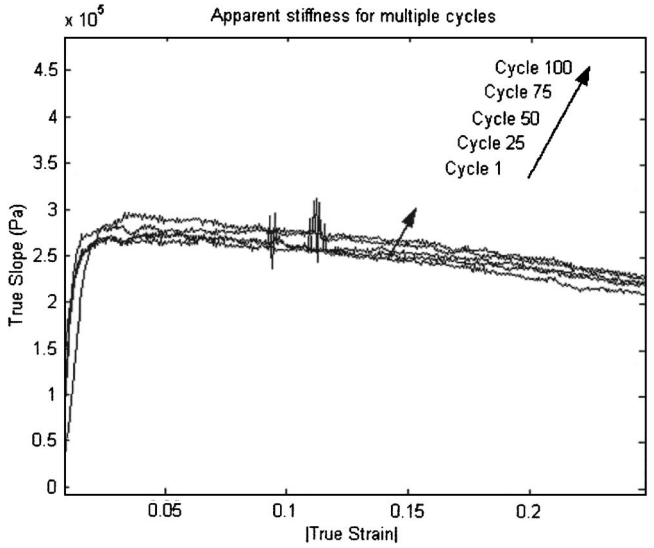

FIG. 21. Apparent stiffness increases significantly over 100 cycles with soapy water interface.

V. DISCUSSION

The squeeze film effect associated with conventional liquid lubricants is a complex phenomenon that depends on: the viscosity of the fluid, the size of the sample, the surface of the sample, the strain rate, and load direction (loading versus unloading). The thickness of the film typically causes an offset in the data which can be difficult to quantify since the transition is not necessarily sharp. In general, oil yields lower apparent material stiffnesses than any other case, but this is likely due to the initial squeeze film effect of the oil itself. As strains increase, air bearings should theoretically yield the lowest apparent stiffness if they were behaving ideally, indicating there might be some residual friction in the system from sample asperities or edges making physical contact.

For noncyclic testing, air bearings perform similarly to soapy water, evidenced by almost identical stiffness profiles. Experimental data have shown, however, that air bearing performance is better at lower loads and soapy water is better at higher loads. This is attributed to the friction arising from contact with the sample under decreasing gaps. Again, better surface finish and/or higher permeability ratio would appear to correct this condition.

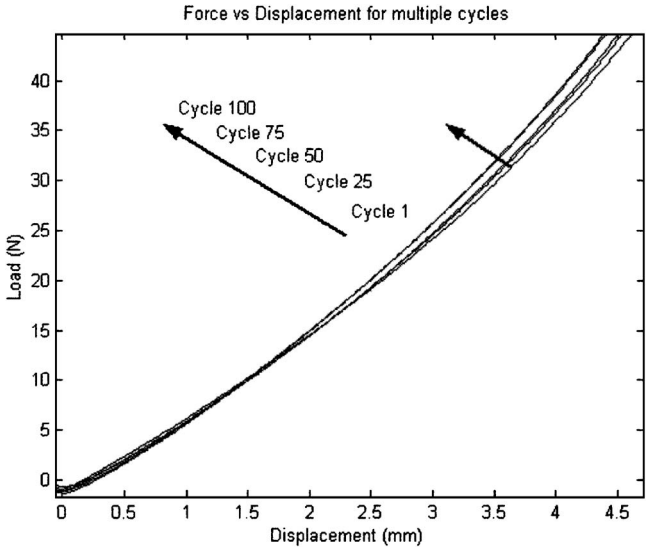

FIG. 20. Stress-strain curve showing slow relative hardening with increasing cycles with soapy water interface.

The performance of air bearing testing improves with increasing flatness, smoothness, and aspect ratio. These parameters affect the amount of contact the sample makes with the bearing. The greater the contact between the sample surface and the bearing, the greater the friction. As a consequence, when the surface roughness increases, air bearing performance becomes less predictable.

Based on these observations, there appear to be significant advantages associated with the use of air bearing platens for material compression tests:

(1) The results are more repeatable (for instance, soapy water can be mixed at varying ratios of water to soap, affecting both the squeeze film and friction coefficient).
(2) Air bearings have the lowest "settling strain," thus they cause less of an offset in the data.
(3) The settling strain is sharply defined for air bearings.
(4) Chance of material properties being changed due to chemical reaction or material swelling (due to contact with liquids) is minimal.
(5) The air bearing interface does not change during cyclic testing. This allows for more confidence in cycle dependent test results.
(6) Air bearings are clean, easy to use, and work for a variety of samples.

There are several opportunities to continue this investigation. The performance of air bearings under long-term test conditions such as stress relaxation and creep tests should be investigated. Also, the friction mechanism involved for very rough surfaces still needs further quantitative evaluation. High permeability ratio bearings should be specifically designed and tested to increase the maximum roughness under which air bearings give adequate performance.

ACKNOWLEDGMENTS

The authors would like to thank Asha Balakrishnan for support and advice with this project, Professor Simona Socrate and Dr. Nannaji Saka with whom we had helpful discussions, and Professor Mary Boyce for access to the experimental equipment.

[1] A. Slocum, M. Basaran, R. Cortesi, and A. J. Hart, J. Int. Soc. Precision Eng. Nanotechnol. **27**, 382 (2003).
[2] S. H. Crandall, N. C. Dahl, and T. J. Lardner, *An Introduction to Mechanics of Solids*, 2nd ed. (McGraw–Hill, New York, 1978).
[3] A. H. Slocum, *Precision Machine Design* (SME, Dearborn, MI, 1992).
[4] J. S. Plante, J. Vogan, T. El-Aguizy, and A. H. Slocum, Precis. Eng. (accepted).
[5] R. Brown, *Physical Testing of Rubber*, 3rd ed. (Chapman and Hall, London, 1996).
[6] New Way Precision, ⟨http://www.newwayprecision.com/drawingpages/flatpages/s124001.html⟩, Data Sheets (January 2004).
[7] Texture Technologies, ⟨http://www.texturetechnologies.com/TAXTPlus_Texture_Analyzer.html⟩, Instrument Specification Sheet (January 2004).
[8] A. N. Gent and P. B. Lindley, Proc. Inst. Mech. Eng. **173**, 111 (1959).